JMEPEG (2003) 12:609-622

Optimization of Process Parameters for the Manufacturing of Rocket Casings: A Study Using Processing Maps

G.S. Avadhani

(Submitted 19 June 2003)

Maraging steels possess ultrahigh strength combined with ductility and toughness and could be easily fabricated and heat-treated. Bulk metalworking of maraging steels is an important step in the component manufacture. To optimize the hot-working parameters (temperature and strain rate) for the ring rolling process of maraging steel used for the manufacture of rocket casings, a systematic study was conducted to characterize the hot working behavior by developing processing maps for γ-iron and an indigenous 250 grade maraging steel. The hot deformation behavior of binary alloys of iron with Ni, Co, and Mo, which are major constituents of maraging steel, is also studied. Results from the investigation suggest that all the materials tested exhibit a domain of dynamic recrystallization (DRX). From the instability maps, it was revealed that strain rates above 10 s^{-1} are not suitable for hot working of these materials. An important result from the stress-strain behavior is that while Co strengthens γ-iron, Ni and Mo cause flow softening. Temperatures around 1125 °C and strain rate range between 0.001 and 0.1 s^{-1} are suitable for the hot working of maraging steel in the DRX domain. Also, higher strain rates may be used in the meta-dynamic recrystallization domain above 1075 °C for high strain rate applications such as ring rolling. The microstructural mechanisms identified from the processing maps along with grain size analyses and hot ductility measurements could be used to design hot-working schedules for maraging steel.

Keywords gamma iron, hot workability/ductility, kinetic analysis, maraging steel, processing maps

1. Introduction

Mechanical processing is an essential step in shaping materials into engineering components, which require dimensional accuracy as well as specified microstructures and mechanical properties. Steels are primarily processed[1] by bulk metal working methods using rolling, forging or extrusion, which are generally conducted at elevated temperatures (in the austenitic range) in order that large strains may be imposed in a single step of operation without the onset of fracture. Among all the mechanical processing methods, the bulk metal working stage is considered to be of primary importance for two reasons. First, in this stage, major microstructural changes occur, and these have a profound influence on subsequent processing steps. Second, in view of the large tonnage of material being processed by bulk metalworking, any improvement in processing techniques has a multiplying effect on the overall productivity in manufacturing. Thus, considerable effort has gone into developing techniques for the design and optimization of bulk metal working processes. The ultimate objective is to manufacture merchant products or components with controlled microstructure and properties, without macro or microstructural defects, on a repeatable basis in a manufacturing environment.

G.S. Avadhani, Principal Research Scientist, Department of Metallurgy, Indian Institute of Science, Bangalore 560 012 India. Contact e-mail: gsa@metalrg.iisc.ernet.in.

Hitherto, processes are developed using trial and error techniques, which are expensive as well as time consuming and may not always lead to a successful solution or optimization, particularly for advanced materials like superalloys, intermetallics, and high strength materials like maraging steel. In recent years, however, the trial and error techniques are replaced by modeling techniques, which are developed on the basis of science based principles. The processing map approach[2] developed on the basis of the dynamic materials model[3] has been found to be a very useful tool for understanding the hot deformation mechanisms in a variety of materials and optimize the hot workability. In this approach, the power dissipation efficiency η of the material is defined as

$$\eta = \frac{2m}{m+1}, \quad \text{(Eq 1)}$$

where m is the strain rate sensitivity of flow stress. The variation of η with temperature and strain rate represents the characteristics of power dissipation occurring through microstructural changes in the workpiece, which constitutes a power dissipation map. A continuum instability criterion[2] developed on the basis of extremum principles of irreversible thermodynamics, which is given by

$$\xi(\dot{\varepsilon}) = \frac{\partial \ln(m/m+1)}{\partial \ln \dot{\varepsilon}} + m < 0 \quad \text{(Eq 2)}$$

is used to delineate the regimes of flow instability. The instability parameter $\xi(\dot{\varepsilon})$ is evaluated as a function of temperature

and strain rate and plotted to obtain an instability map. It is superimposed onto the power dissipation map to obtain a processing map.

The characteristics of hot working of γ iron has been studied in the past using hot tensile and torsion tests.[4,5] However, scanty data is available on hot working of steels over a wide range of temperature and strain rate and on the mechanism of dynamic recrystallization (DRX) during hot working. The objective of the present investigation is to carry out a systematic study to characterize the hot working domain by developing processing maps for γ-iron, binary alloys of iron with Ni, Co and Mo additions, which are major constituents of maraging steel. Also, processing map for an indigenous 250 grade maraging steel was produced over wide temperature and strain rate ranges with a view to optimize process parameters of the ring rolling, which is used for manufacturing rocket casings.

2. Experimental Procedure

The chemical composition and prior history of all the materials used in this investigation are given in Table 1. Cylindrical specimens of diameter 10 mm and height 15 mm were used for hot compression testing. Care was taken to obtain closely parallel load bearing surfaces for the specimen. In addition, grooves were provided on these surfaces so that effective lubrication (using a borosilicate glass lubricant) was ensured during compression. The temperature of the specimen was monitored with the aid of a chromel-alumel thermocouple embedded in a 0.8 mm diameter hole machined at half the specimen height. This thermocouple was also used to monitor the adiabatic temperature rise during deformation. A computer-controlled servo-hydraulic testing machine (DARTEC, Bangalore, India) was used for the hot compression tests. The ma-

Table 1 Chemical Composition, Initial Grain Size and Prior Thermomechanical Processing of the Materials Used in the Study

Material	C	Mn	S	P	Ni	Co	Mo	Ti	Al	Cr	Si	B	Zr	Fe	Initial Grain Size, μm	Prior History
γ-Fe (Armco iron)	0.007	<0.03	0.005	0.003	…	…	…	…	…	…	…	…	…	Bal.	118	Forged at 900 °C/annealed at 750 °C for 2 hrs/furnace cooled
Fe-5Ni	0.007	<0.03	0.005	0.003	5	…	…	…	…	…	…	…	…	Bal.	125	—do—
Fe-5Co	0.007	<0.03	0.005	0.003	…	5	…	…	…	…	…	…	…	Bal.	125	Hot forged at 700 °C/annealed at 875 °C for 2 hrs/furnace cooled
Fe-5Mo	0.007	<0.03	0.005	0.003	…	…	5	…	…	…	…	…	…	Bal.	125	Hot forged and annealed
Maraging Steel, M250	0.016	0.07	…	…	17.2	7.3	4.7	0.32	0.15	0.05	0.05	0.002	0.002	Bal.		Hot rolled

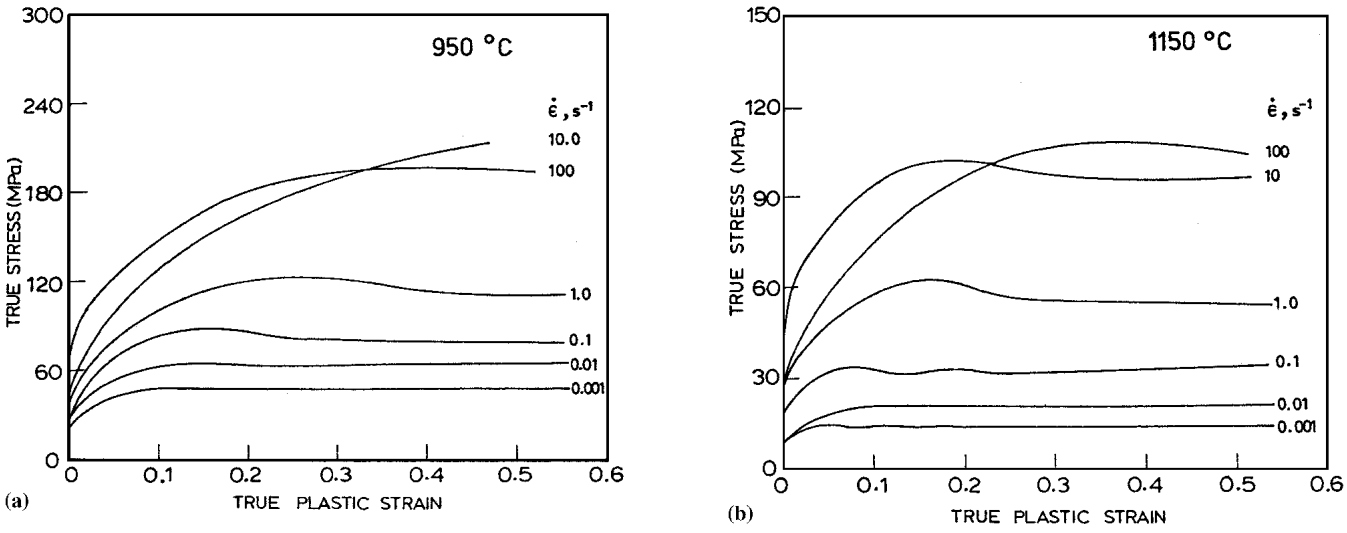

Fig. 1 True stress-true plastic strain curves obtained at different strain rates for γ-iron at **(a)** 950 °C and **(b)** 1150 °C

chine was equipped with an exponentially decaying actuator speed, enabling constant true strain rates in the range 0.001-100 s^{-1} to be imposed on the specimen. Isothermal tests were conducted by surrounding the specimen, platens, and push rods with a resistance furnace having silicon carbide heating elements. The temperature was controlled to within ±2 °C. The adiabatic temperature rise was recorded using a Nicolet transient recorder (Bangalore, India). The tests were conducted over a temperature range of 950-1200 °C at intervals of 50 °C for various strain rates ranging from 0.001-100 s^{-1}. In each test, the specimens were compressed to about half their original height and the load-stroke data were obtained. The load-displacement curves were converted into true stress-true plastic strain curves using standard equations and a personal computer. The flow stress data as functions of temperature, strain rate, and strain were obtained from these curves and used to construct the power dissipation map. The log (flow stress) versus log (strain rate) data were fitted using a cubic spline and strain rate sensitivity m was calculated as a function of strain rate. This was repeated for various temperatures investigated. The efficiency of power dissipation through microstructural changes was then calculated as a function of temperature and strain rate and plotted as an iso-efficiency contour map. Similarly, the instability parameter was plotted as a function of temperature and strain rate to get the instability map, which was superimposed on the power dissipation map to get the processing map for the materials investigated.

3. Results and Discussion

3.1 γ-Iron

3.1.1 Stress-Strain Behavior. Typical true stress-true plastic strain curves obtained on γ-iron at 950 and 1150 °C and different strain rates are given in Fig. 1(a) and 1(b), respectively. At strain rates lower than 1 s^{-1}, the stress-strain curves exhibited flow stress maxima followed by a steady-state be-

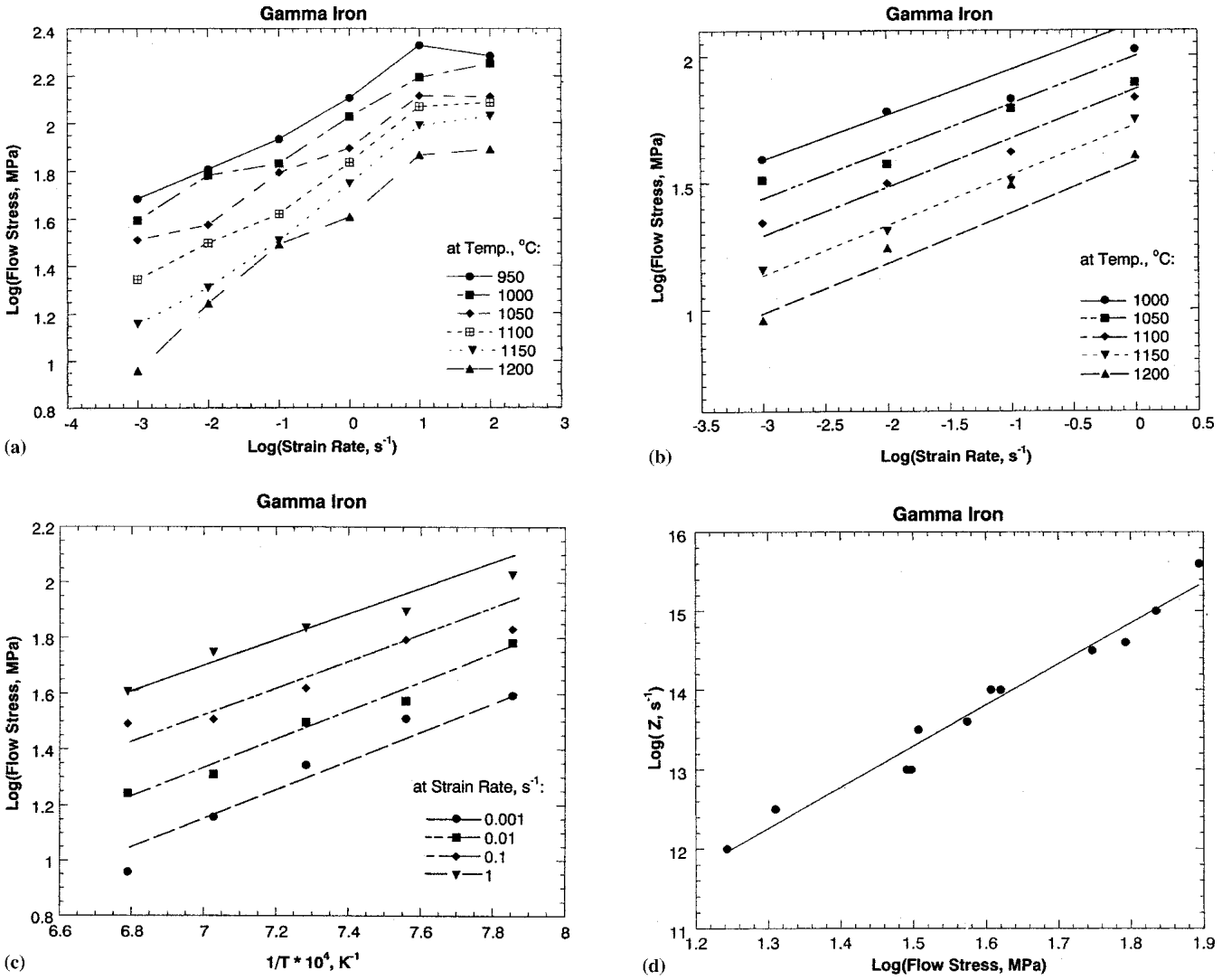

Fig. 2 Kinetic analysis of flow stress data on γ-iron: **(a)** plot of log $\dot{\varepsilon}$ versus log σ in the entire range of test temperature and strain rate, **(b)** in the range 1000-1200 °C and 0.001-1.0 s^{-1}, **(c)** Arrhenius plot of $1/T$ versus log σ, and **(d)** plot of log(σ) versus log(Z) in the temperature range 1000-1200 °C and strain rate range 0.001-1.0 s^{-1}

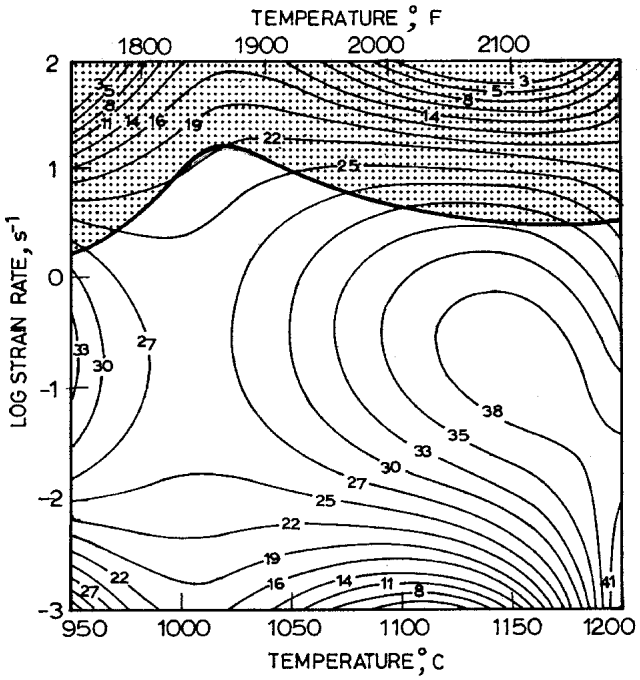

Fig. 3 Processing map obtained for γ-iron at a strain of 0.3. Contour numbers represent percent efficiency of power dissipation. Shaded region corresponds to flow instability

havior. However, at higher temperatures and lower strain rates, multiple peaks occurred before a steady-state (Fig. 1b) is reached. Flow softening or oscillations in stress-strain curves are indicative of either dynamic recrystallization (DRX) or flow instability. However, the steady-state condition reached after certain strain is caused by DRX. This is further confirmed by other methods of material modeling. At strain rates higher than 10 s^{-1}, the flow curves have crossed over, the strain at which it occurred being lower at higher temperatures. The flow stress data (corrected for adiabatic temperature rise) at different temperatures, strain rates, and strains are given in Table 1.

3.1.2 Kinetic Analysis. The kinetic rate equation relating the flow stress with temperature and strain rate is given by[6]

$$\dot{\varepsilon} = A\,\sigma^{n}\exp[-Q/RT], \qquad \text{(Eq 3)}$$

where $\dot{\varepsilon}$ is strain rate, A is a constant, σ is flow stress, n is the stress exponent, Q is the activation energy for hot deformation, R is the gas constant, and T is the absolute temperature. A plot of log σ versus log $\dot{\varepsilon}$ is shown in Fig. 2(a). If the kinetic rate equation is obeyed over the entire range of temperature, strain rate, a linear relationship is expected, and the slope of such a line is equal to n, the stress exponent. However, Fig. 2(a) shows that n is strain rate and temperature dependent. Considering the data over a limited range of temperature (1000-1200 °C) and strain rate (0.001-1.0 s^{-1}), the log σ versus log $\dot{\varepsilon}$ plot in Fig. 2(b) shows that the kinetic rate equation is obeyed and the value of n is 4.5. For the same range of test parameters, Arrhenius plot of log σ versus $1/T$ is shown in Fig. 2(c), which yields an apparent activation energy of 395 kJ/mol. This is much higher than the activation energy of self-diffusion in γ-iron (282 kJ/mol).[7] To confirm whether the rate equation is

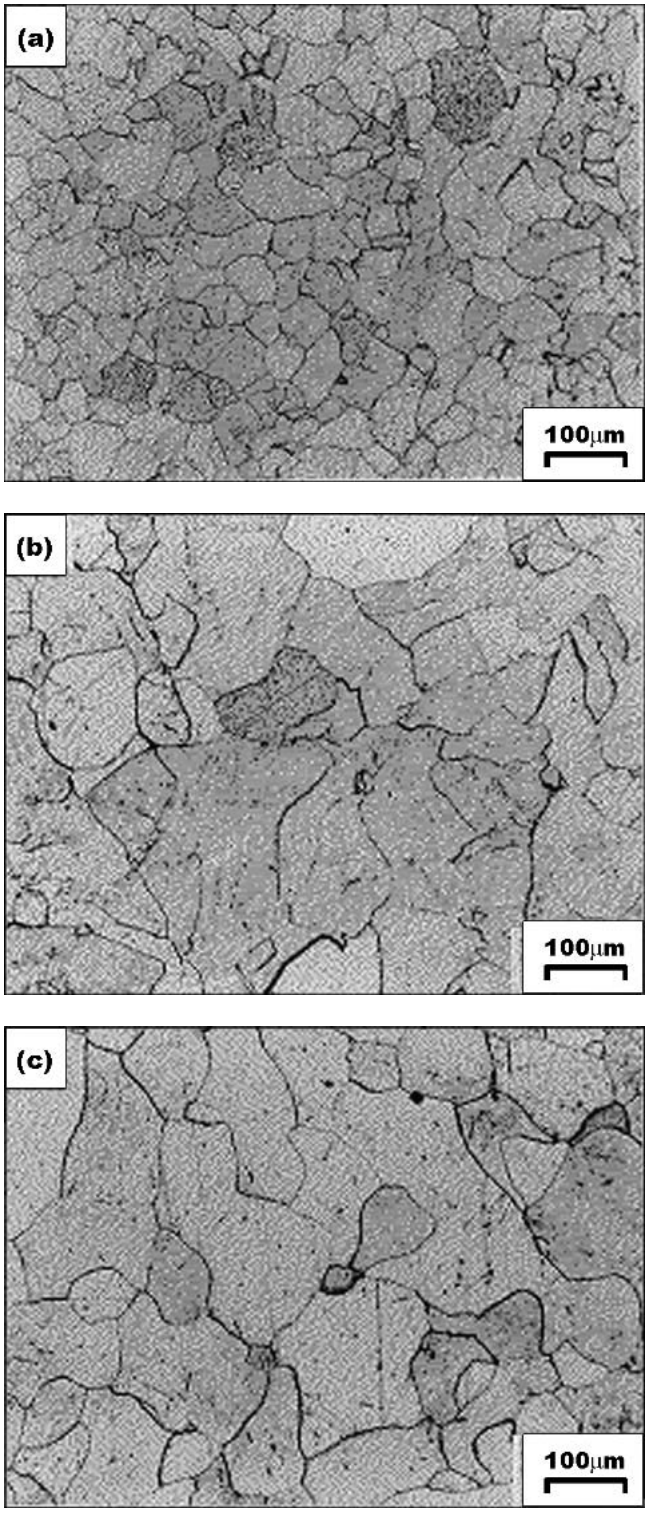

Fig. 4 Microstructures obtained on γ-iron specimens deformed at **(a)** 1050 °C/0.1 s^{-1}, **(b)** 1150 °C/0.1 s^{-1}, and (c) 1200 °C/0.1 s^{-1}, in the DRX domain

obeyed, the variation of Zener-Hollomon parameter Z given by

$$Z = \dot{\varepsilon}\exp\left(\frac{Q}{RT}\right) \qquad \text{(Eq 4)}$$

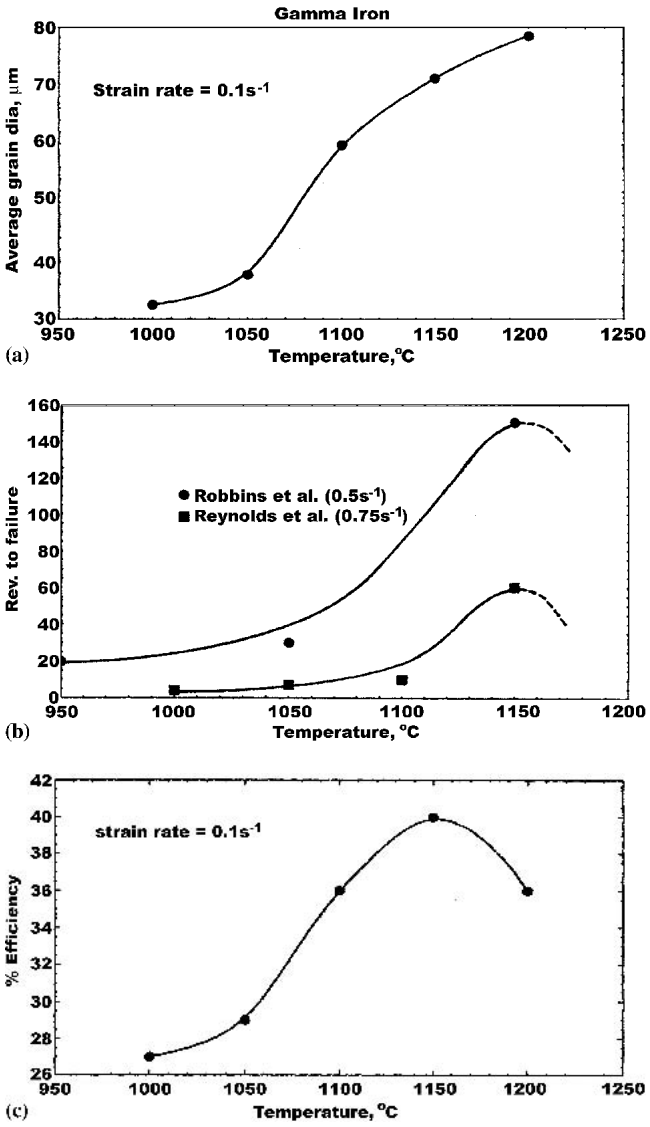

Fig. 5 **(a)** Variation of average grain diameter, **(b)** torsional ductility, and **(c)** efficiency of power dissipation with temperature for γ-iron in the DRX domain

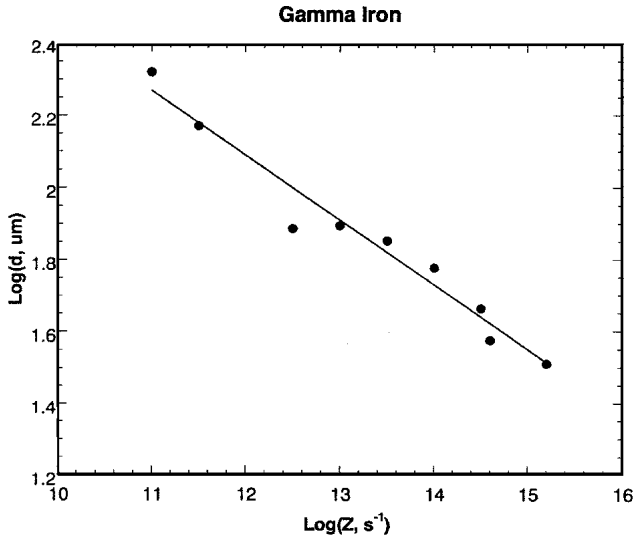

Fig. 6 Variation of average grain diameter (*d*) with the Zener-Hollomon parameter (Z) in the DRX domain of γ-iron

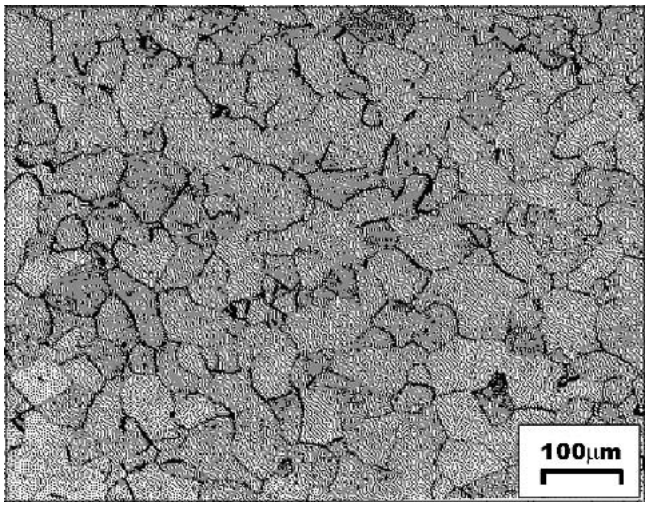

Fig. 7 Microstructure obtained on γ-iron specimen deformed at 950 °C/0.1s^{-1}, exhibiting post deformation recrystallization after dynamic recovery

is plotted against log σ in Fig. 2(d). The linear relationship exhibited by this variation confirms the applicability of the kinetic analysis.

3.1.3 Processing Map. A processing map is obtained by superimposing the instability map on the efficiency map of γ-iron at 0.3 strain is shown in Fig. 3. The general features of the maps are similar for other strains indicating that the influence of strain on the hot deformation mechanism is not significant.

The processing map for γ-iron exhibits two domains: (i) a domain in the temperature range 1000-1200 °C and strain rate range 0.01-2 s^{-1} with a maximum η of 38% occurring at 1150 °C and 0.3 s^{-1} and (ii) a domain in the temperature range 950-1000 °C and strain rate range 0.01-1 s^{-1} with a peak efficiency of 33% occurring at 950 °C and 0.3 s^{-1}. Referring to domain (i), typical microstructures recorded on the specimens deformed at 1050, 1150, and 1200 °C and a strain rate of 0.1 s^{-1} are shown in Fig. 4. These microstructures exhibit wavy grain boundaries typical of DRX. The waviness occurs since the time available during cooling of the deformed specimen is insufficient to form equilibrium grain boundary configuration (namely, 120° triple junction with straight grain boundaries). The variation of average grain diameter with temperature at a strain rate of 0.1 s^{-1} in this domain is shown in Fig. 5(a), which exhibits a sigmoidal variation, typical of a nucleation and growth process, like DRX. Such microstructural features of DRX in γ iron were also reported by Reynolds and Tegart.[5] The variation of torsional ductility with temperature for γ-iron as measured by Robbins et al.[4] at a strain rate of 0.5 s^{-1} and by Reynolds and Tegart[5] at a strain rate of 0.75 s^{-1} are shown in Fig. 5(b). These curves show a sharp increase in ductility above 1050 °C to reach a maximum value at 1150 °C. The

variation of efficiency with temperature at a strain rate of 0.1 s^{-1} in the DRX domain is shown in Fig. 5(c) for comparison. It may be noted that the temperature for peak efficiency matches with that of the ductility. On the basis of the microstructural observations, grain size variation, and ductility measurements, this domain is interpreted to represent DRX process. The conditions for optimum hot workability of γ-iron are 1150 °C and 0.3 s^{-1}. In hot working, the variation of grain size with the processing parameters is generally correlated with *Z*. Using a value of 395 kJ/mol for *Q*, the *Z* values have been calculated and plotted against average grain diameter (*d*) in Fig. 6. The relation may be expressed by the following equation

$$\log(d) = 4.2 - 0.18 \log (Z) \quad \text{(Eq 5)}$$

This equation is useful for predicting the grain size that develops during hot working of this material.

The microstructure of the specimen deformed under peak efficiency conditions of the second domain (950 °C/0.1 s^{-1}) is shown in Fig. 7, which represents a relatively fine-grained equiaxed microstructure. This is indicative of a process of dynamic recovery followed by post deformation recrystallization during cooling of specimen from deformation temperature to room temperature.

The regime of flow instability as per the criterion given by Eq 2 is shown as shaded area in the processing map (Fig. 3). This regime occurs in the entire test temperature range of 950-1200 °C and strain rates above 10 s^{-1}. It may be noted that the crossover of stress-strain curves has occurred in this regimen (Fig. 2a). In view of the changes in the microstructure that occur during cooling, it is not feasible to record the exact manifestations of the flow instabilities occurring under high strain rate, hot-conditions. However, some signatures of these instabilities are retained in the microstructure as observed at

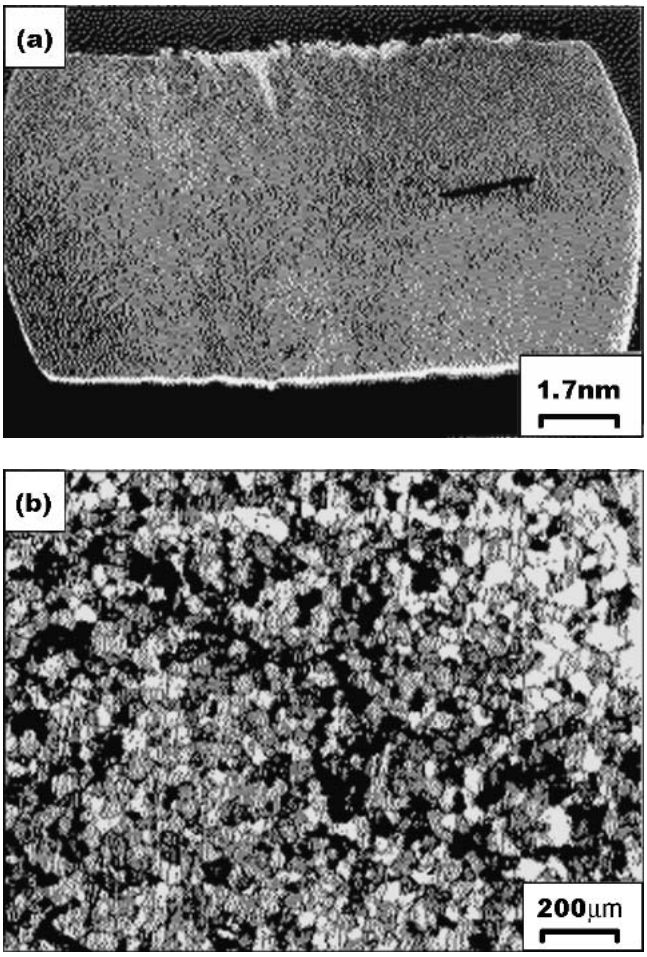

Fig. 8 **(a)** Macrostructure and **(b)** microstructure obtained on γ-iron specimen deformed at 950 °C/100 s^{-1} in the instability regimen (the compression axis is vertical)

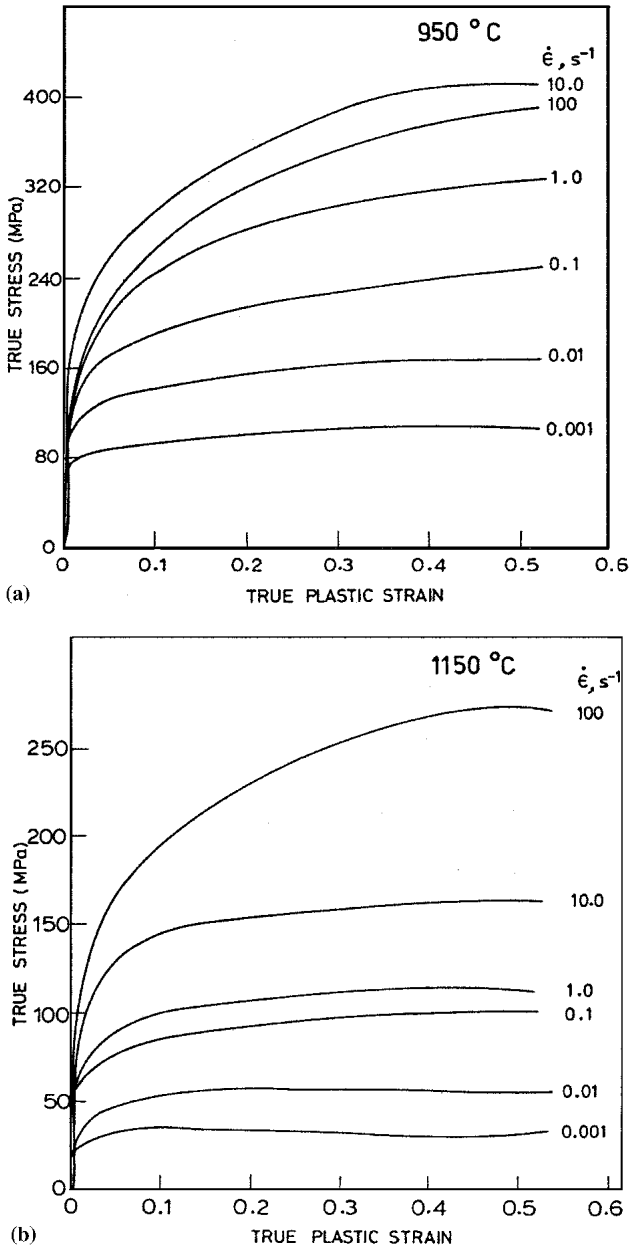

Fig. 9 True stress-true plastic strain curves obtained at different strain rates for maraging steel at **(a)** 950 °C and **(b)** 1150 °C

Table 2 Flow Stress Values (in MPa) of γ-Iron at Different Temperatures and Strain Rates for Various Strains (Corrected for Adiabatic Temperature Rise)

Strain	Strain Rate, s^{-1}	Temperature, °C					
		950	1000	1050	1100	1150	1200
0.1	0.001	49.1	38.4	33.1	21.9	15.0	8.6
	0.010	64.6	56.5	39.6	32.4	20.8	18.5
	0.100	85.8	69.5	62.5	47.9	32.7	34.9
	1.000	104.7	84.9	77.5	62.7	56.7	48.1
	10.00	161.8	111.9	98.0	94.6	92.7	61.2
	100.0	129.6	121.7	112.3	84.9	74.4	53.3
0.2	0.001	49.1	39.0	33.4	21.9	14.7	9.1
	0.010	64.6	59.5	37.8	32.3	20.5	17.8
	0.100	93.4	69.8	62.6	42.1	32.9	31.9
	1.000	127.2	104.9	85.6	73.1	60.7	47.5
	10.00	197.5	141.4	119.7	114.7	102.3	73.2
	100.0	170.4	156.5	143.8	109.9	97.0	67.0
0.3	0.001	48.3	39.3	32.4	22.1	14.4	9.1
	0.010	64.1	60.5	37.5	31.4	20.4	17.5
	0.100	85.8	67.7	62.1	41.7	32.1	31.0
	1.000	127.6	106.2	78.3	68.4	55.8	40.5
	10.00	214.0	156.1	130.0	117.0	97.4	73.3
	100.0	192.8	178.6	162.4	122.0	106.6	77.3
0.4	0.001	48.0	39.8	32.5	22.8	14.4	9.3
	0.010	64.9	61.4	37.3	31.9	20.9	17.5
	0.100	84.1	66.8	61.6	41.8	33.5	30.6
	1.000	119.6	100.1	76.8	67.2	54.6	39.2
	10.00	219.6	160.7	128.1	111.4	96.7	70.0
	100.0	210.2	194.1	176.2	128.2	108.0	81.9
0.5	0.001	48.6	41.1	33.0	23.5	14.5	9.3
	0.010	66.2	62.1	37.6	32.1	21.7	17.4
	0.100	83.8	66.6	61.8	42.2	33.4	30.9
	1.000	116.9	97.3	78.0	67.7	54.2	37.3
	10.00	226.9	159.1	122.4	103.7	98.1	72.0
	100.0	220.0	200.9	181.0	125.0	103.8	81.2

Table 3 Flow Stress Values (in MPa) of Maraging Steel at Different Temperatures and Strain Rates for Various Strains (Corrected for Adiabatic Temperature Rise)

Strain	Strain Rate, s^{-1}	Temperature, °C						
		900	950	1000	1050	1100	1150	1200
0.1	0.0010	127.1	93.0	71.9	54.1	46.1	35.3	27.7
	0.010	214.0	140.2	113.7	87.6	69.0	53.2	39.0
	0.100	245.6	190.0	157.1	120.7	106.2	85.2	67.6
	1.000	422.4	242.6	231.5	171.9	141.7	104.6	78.5
	10.00	383.2	315.2	255.4	220.3	179.3	149.4	124.9
	100.0	273.9	266.5	244.9	231.0	195.6	192.9	138.6
0.2	0.001	138.5	100.6	78.1	57.6	46.1	33.3	27.5
	0.010	217.5	155.0	124.6	98.4	78.4	57.5	40.9
	0.100	266.3	211.9	174.6	134.0	117.6	94.0	74.2
	1.000	385.8	280.6	266.5	193.5	157.6	113.7	83.3
	10.00	384.7	358.3	301.9	260.1	206.9	163.0	132.4
	100.0	324.7	320.9	298.1	278.0	232.2	228.2	154.3
0.3	0.001	145.1	105.4	79.5	55.7	44.9	33.0	26.1
	0.010	219.3	163.1	129.3	101.8	77.7	56.9	38.7
	0.100	280.9	225.1	186.2	139.1	122.5	98.0	76.1
	1.000	352.8	303.2	287.3	207.2	166.7	118.9	86.7
	10.0	368.2	382.2	325.8	279.3	219.7	172.1	139.1
	100.0	344.8	352.4	325.8	298.5	254.7	252.9	164.8
0.4	0.001	148.9	107.6	78.4	55.4	47.3	32.5	26.2
	0.010	220.0	167.8	129.3	100.8	75.2	56.4	39.1
	0.100	289.2	238.1	191.5	140.7	124.5	99.1	80.5
	1.000	332.6	321.6	305.2	211.3	171.6	120.6	88.0
	10.00	366.8	409.0	348.4	297.2	226.9	175.3	141.1
	100.0	375.0	374.8	343.1	311.1	263.3	262.5	177.0
0.5	0.001	154.4	106.6	80.6	57.2	49.5	34.3	27.6
	0.010	221.9	169.6	128.4	101.8	75.3	56.6	41.2
	0.100	297.6	256.1	195.1	141.0	128.2	103.2	85.6
	1.000	320.6	344.1	329.6	215.8	172.0	120.4	89.4
	10.00	376.8	436.9	372.1	313.9	233.7	177.9	143.5
	100.0	396.5	386.6	350.5	309.1	260.5	260.2	193.3

room temperature after cooling. These are shown macroscopically in Fig. 8(a) and microscopically in Fig. 8(b). The microstructure reveals post deformation recrystallization (Fig. 8b) in flow localization bands observable at very low magnification (Fig. 8a). The entire instability regime has to be avoided while processing γ iron to avoid undesirable microstructures.

3.2 Maraging Steel

3.2.1 Stress-Strain Behavior. Typical true stress-true plastic strain curves obtained on maraging steel at temperatures of 950 and 1150 °C and at different strain rates are given in Fig. 9(a) and 9(b), respectively. The flow curves at lower temperatures (950 °C) exhibited steady-state behavior at lower strain rates (<1 s^{-1}) and strain hardening type of behavior at higher strain rates. At 1150 °C, the curves depicted steady state behavior at strain rates lower than 10 s^{-1} and flow softening followed by steady state at 0.001 s^{-1}. The latter behavior is indicative of DRX. The flow stress data corrected for adiabatic temperature rise at different temperature, strain rates and strains are given in Table 2 and 3.

3.2.2 Kinetic Analysis. A plot of logσ versus log $\dot{\varepsilon}$ for the entire range of temperature and strain rate used in this investigation is shown in Fig. 10(a). The data show that the kinetic rate equation (Eq 3) is not obeyed over the entire range of strain rate since instead of a straight line, a curve is obtained indicating that the stress exponent n is strain rate dependent. However, over a limited range of strain rate (0.001-0.1 s^{-1}), a reasonable linear fit occurs (Fig. 10b) and this yields a value of 4.2 for the stress exponent. Arrhenius plot relating log σ versus $(1/T)$ at strain rates of 0.001 and 0.01 s^{-1} is shown in Fig. 10(c). At strain rates higher than 0.01 s^{-1}, the data deviated from the kinetic rate equation. The value of apparent activation energy estimated from the slope of these plots is 355 kJ/mol, which is higher than the activation energy for self-diffusion in γ-Fe (286 kJ/mol)[7] or for the diffusion of Mo in γ-Fe (252 kJ/mol).[8] The Z parameter (Eq 4) is calculated by using a value of 355 kJ/mol for Q and plotted against log σ in Fig. 10(c). The plot shows that the kinetic rate equation is obeyed in the limited strain rate range considered above for the kinetic analysis.

3.2.3 Processing Map. The processing map obtained at a strain of 0.3, for the 250 grade maraging steel material is shown in Fig. 11. The general features of the maps for other strains are similar, indicating that the influence of strain is not significant. The processing map exhibits a single domain in the temperature range 1000-1200 °C and strain rate range 0.001-0.01 s^{-1} with a peak efficiency of 43% occurring at 1125 °C and 0.001 s^{-1}. Typical microstructures recorded on the specimens deformed at 1050, 1150, and 1200 °C, at 0.001 s^{-1} are shown in Fig. 12. Since the material undergoes martensitic transformation on air-cooling from the test temperatures, the features of austenite deformation are masked. However, it is possible to

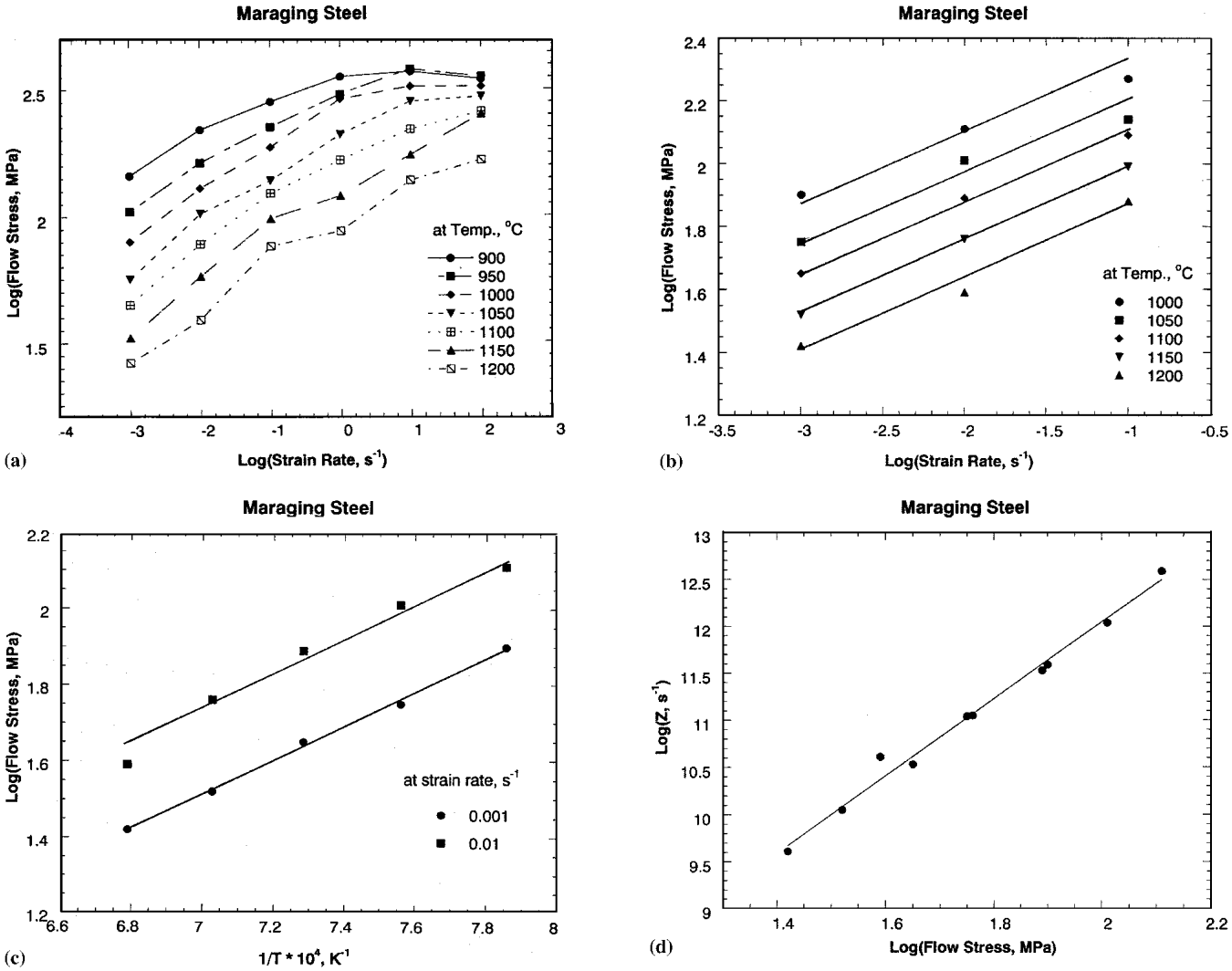

Fig. 10 Kinetic analysis of flow stress data on maraging steel at **(a)** plot of log $\dot{\varepsilon}$ versus log σ for maraging steel in the entire range of test temperature and strain rate, **(b)** in the range 1000-1200 °C and 0.001-0.1 s^{-1}, **(c)** Arrhenius plot of $1/T$ versus log σ, and **(d)** plot of log σ versus log Z in the temperature range 1000-1200 °C and strain rate range 0.001-0.1 s^{-1}

distinguish the prior austenitic boundaries in all the microstructures. The microstructures clearly show that a significant change of prior austenitic grain size occurred as a function of temperature in this domain. The variation of prior austenitic grain size as a function of temperature at a strain rate of 0.001 s^{-1} is shown in Fig. 13(a) and compared with that of the efficiency of power dissipation in Fig. 13(b). At the temperature of peak efficiency, a significant change in the grain size has occurred. Such features are indicative of DRX, which imparts very good workability to the material during hot working. The variation of tensile ductility of the material with temperature at a nominal strain rate of 0.001 s^{-1} is shown in Fig. 13(c). The ductility maximum has occurred at the temperature for the peak efficiency, as is commonly observed in materials undergoing DRX. Beyond this temperature, the occurrence of extensive oxidation has resulted in a drastic drop in the tensile ductility.

The microstructures obtained at the DRX temperature of 1100 °C and at different strain rates of 0.001, 0.01, and 0.1 s^{-1} are shown in Fig. 14. These indicate that the prior austenitic grain size is refined with increase in strain rate, which is again an indication of the DRX process. On the basis of the microstructural observations, grain size variation and the ductility variation, the domain is interpreted to represent DRX process.

The variation of the average grain diameter (d) with Z is shown in Fig. 15, which exhibits a linear relation. The variation of d with Z may be expressed in the form of the equation

$$\log(d) = 4.9 - 0.27 \log(Z) \quad \text{(Eq 6)}$$

The processing map of maraging steel (Fig. 11) exhibits a regime of flow instability up to 1075 °C and at higher strain rates (>1 s^{-1}). At lower temperatures (~900 °C), the instability regimen extends up to strain rate of 0.05 s^{-1}. Typical macrostructure recorded on the specimen deformed at 950 °C/100 s^{-1} is shown in Fig. 16(a), which exhibits localized shear bands. The microstructures recorded at locations inside and outside the band at higher magnification are shown in Fig. 16(b) and

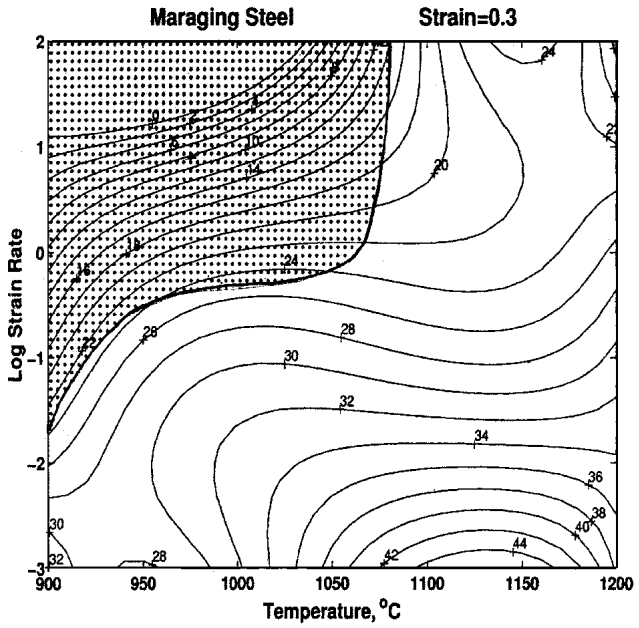

Fig. 11 Processing map obtained for maraging steel at a strain of 0.3. Contour numbers represent percent efficiency of power dissipation. Shaded region corresponds to flow instability.

16(c), which reveal the occurrence of martensitic transformation in these regions during air-cooling. The microstructure is not uniform over the entire specimen as is expected from the occurrence of flow localization.

3.2.4 Ring Rolling of Maraging Steel. One of the important applications of maraging steel is for the manufacture of rocket motor casings using ring-rolling process where hollow billets are ring rolled in the hot working range. In this process, the strain rate encountered increases with deformation and are generally high (1-20 s^{-1}). Microstructural control during processing is essential for achieving the required mechanical properties like fracture toughness. Referring to the processing map obtained on maraging steel (Fig. 11), the strain rates relevant to ring rolling fall much above those where DRX domain has occurred. Under such high strain rate conditions, the material undergoes dynamic recovery if the temperature is above ~1075 °C and exhibits flow instabilities if the temperature is lower than this value. Hence the lower temperature limit is set by the onset of flow instabilities. After dynamic recovery during hot deformation at higher strain rates, the material undergoes post deformation recrystallization during cooling resulting in finer (prior austenitic) grain sizes than those resulting from DRX. This regimen of dynamic recovery followed by static recrystallization is generally referred to as metadynamic recrystallization[9] and the resulting grain size is essentially dependent on the temperature of deformation and the rate of cooling than the deformation strain rate. Such a metadynamic recrystallization could have an affect on the heat treated microstructures. However, the essential requirement for microstructural control in the present case is to avoid the flow instabilities by restricting the temperature from falling below about 1075 °C during ring rolling and this requires careful monitoring of temperature. If the temperature is allowed to fall below this value, flow localization due to adiabatic shear band formation will occur in the product microstructure, which will drastically reduce the dynamic properties including low cycle fatigue and fracture toughness by offering an easy path for crack propagation.

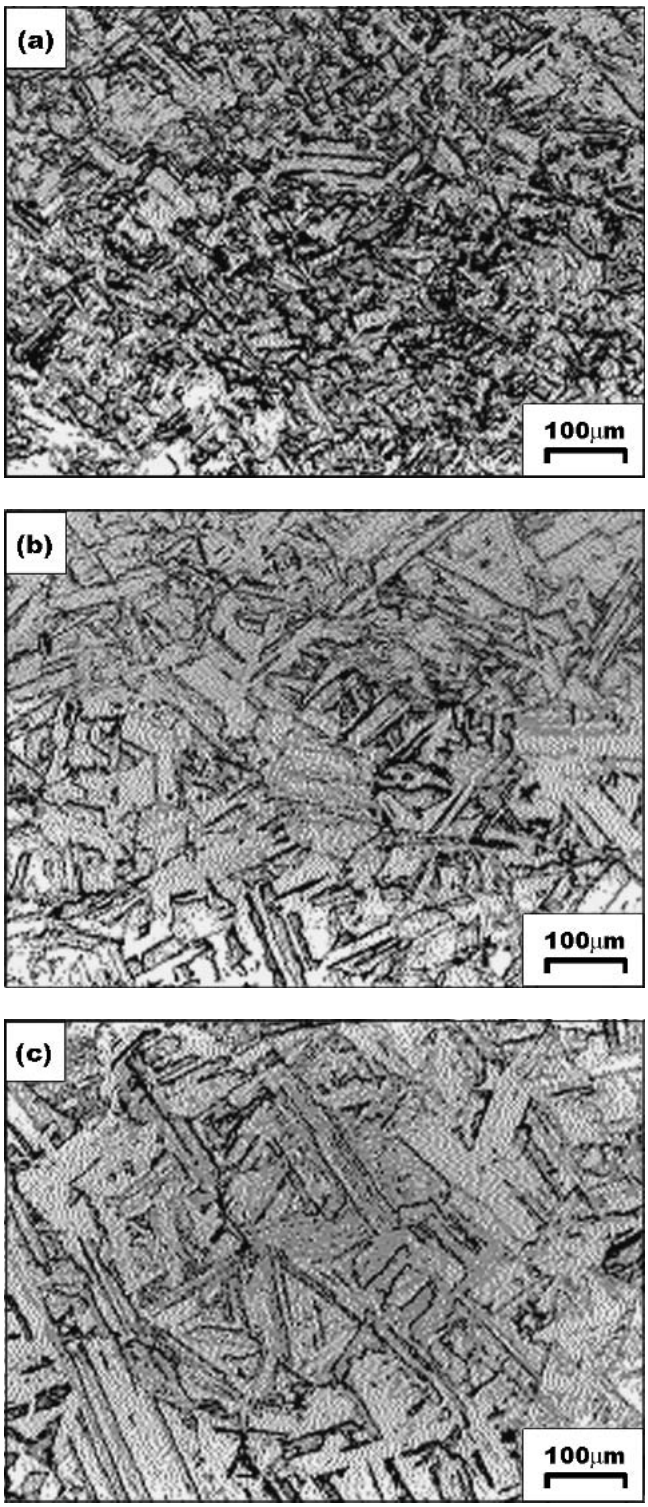

Fig. 12 Microstructures recorded on Maraging Steel specimens deformed at **(a)** 1050 °C, **(b)** 1150 °C, and **(c)** 1200 °C, at 0.001 s^{-1} in the DRX domain

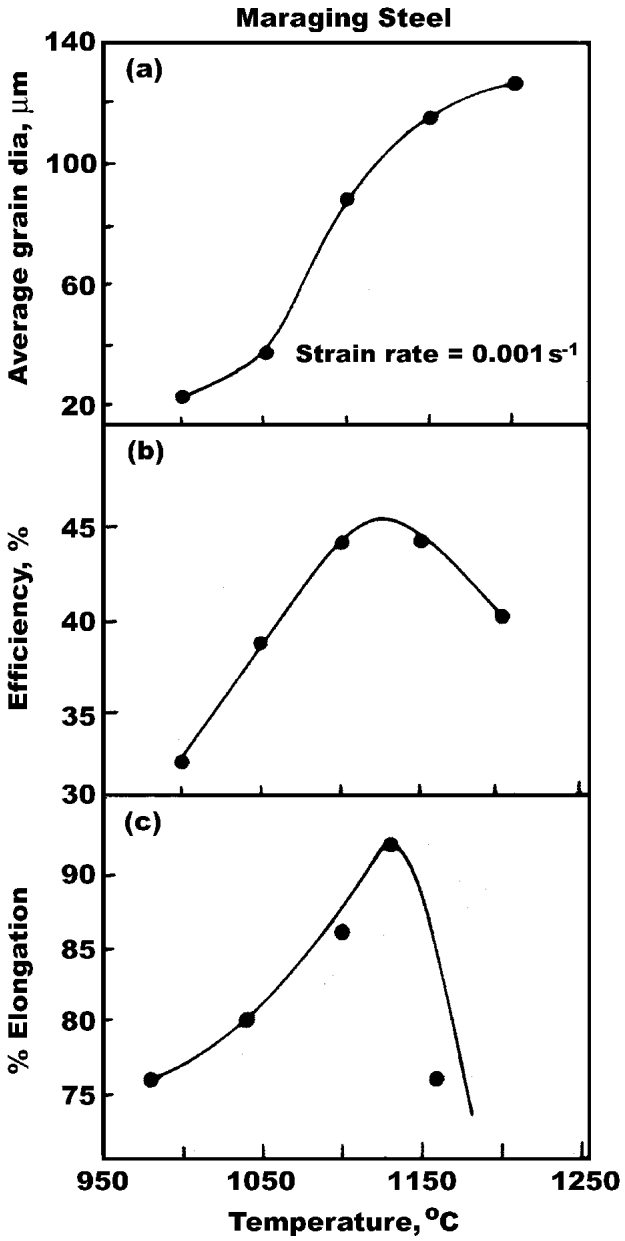

Fig. 13 Maraging steel: **(a)** variation of average grain diameter, **(b)** efficiency of power dissipation, and **(c)** tensile ductility with temperature at 0.001 s^{-1} (DRX domain)

3.3 Effect of Ni, Co, and Mo Additions

The results from the present investigation show that the addition of individual alloying elements has a significant effect on the hot working characteristics of γ-iron.[10] In this section, the effect of the addition of nickel, cobalt, and molybdenum on the stress-strain behavior, kinetic parameters, optimum hot working conditions, mechanisms of hot deformation, and the occurrence of flow instabilities are discussed. This would be useful in understanding the behavior of maraging steel, which has these as the major alloying additions. The processing maps developed for Fe-5Ni, Fe-5Co, and Fe-5Mo alloys are given in Fig. 17, 18, and 19, respectively.

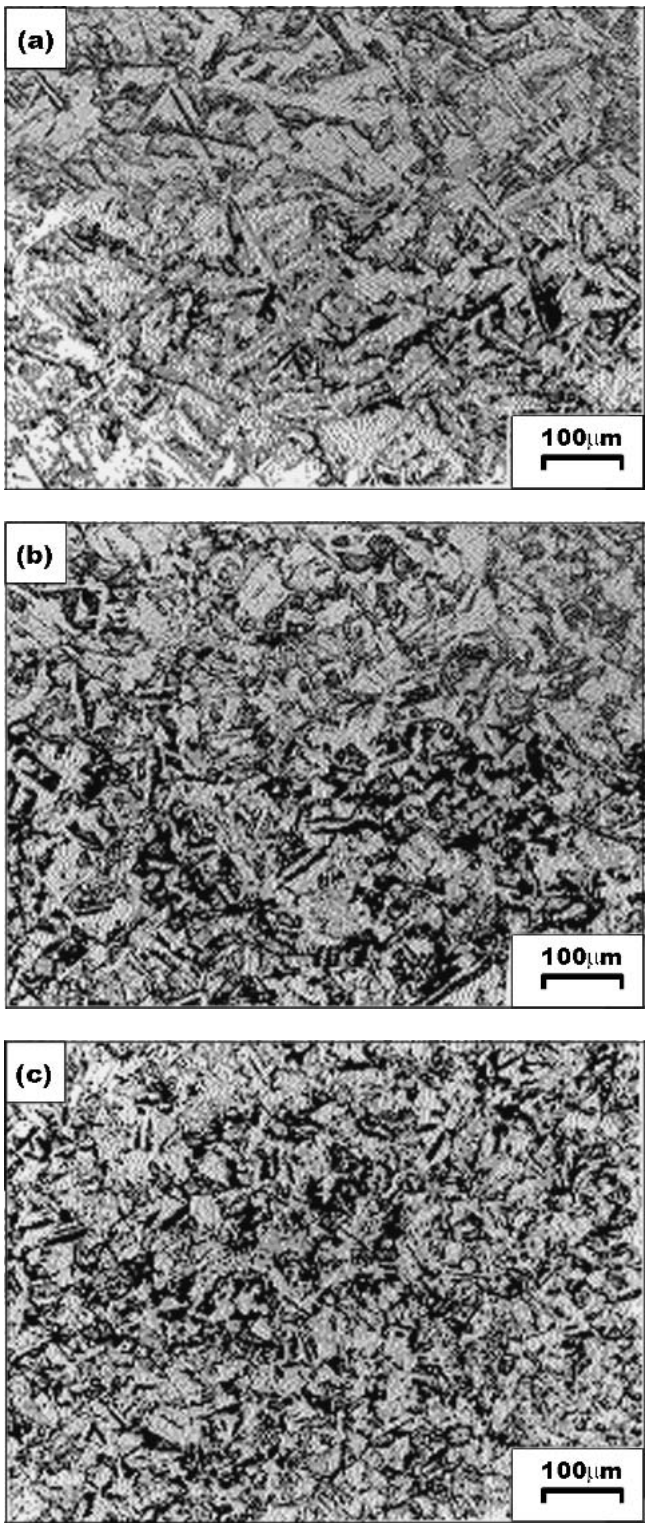

Fig. 14 Microstructures recorded on maraging steel specimens deformed at **(a)** 0.001 s^{-1}, **(b)** 0.01 s^{-1}, and **(c)** 0.1 s^{-1}, at 1100 °C

3.3.1 Stress-Strain Behavior. The true stress-true plastic strain curves obtained on γ-iron, Fe-5Ni, Fe-5Co, Fe-5Mo, and maraging steel (MAS) at 1150 °C and at different strain rates 0.001 and 0.1 s^{-1} are shown in Fig. 20(a) and 20(b), respec-

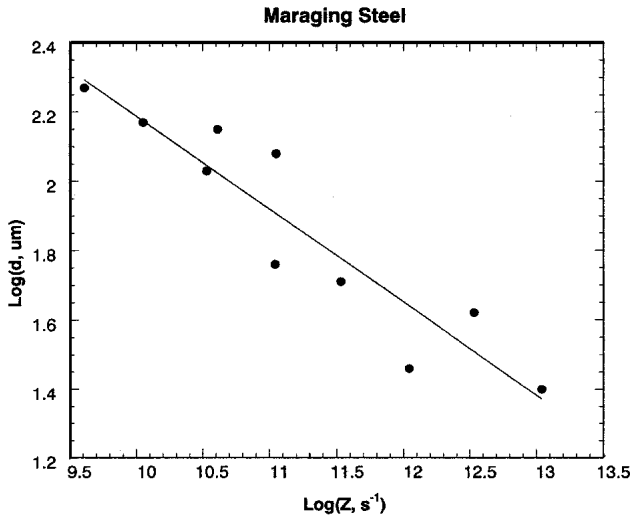

Fig. 15 Variation of average grain diameter (d) with the Zener Hollomon parameter (Z) in the DRX domain for maraging steel

tively. At lower strain rates, γ-iron and Fe-5Co exhibited oscillations before attaining steady-state at larger strains. These oscillations are reduced by increasing the strain rate, and the initial peak in the flow stress occurrs at strains, which are higher at higher strain rates. In contrast, Fe-5Ni, Fe-5Mo, and maraging steel exhibit steady state stress-strain behavior, although in maraging steel, slight flow softening is observed at lower strain rates. All of these materials exhibit DRX at 1150 °C, and the strain rates at which it occurs are higher in γ-iron and Fe-5Co alloy. One of the striking differences exhibited by the binary alloys is that the addition of Ni and Mo lower the flow stress of γ-iron while the addition of Co strengthens the metal. Nickel has an atomic diameter similar to that of iron (0.248 nm), and so not much solid solution strengthening is expected. Molybdenum, on the other hand, has a larger atomic diameter (0.272 nm) and is therefore expected to cause considerable solid solution strengthening. However, the present results do not support this possibility since a decrease in strength is observed. Cobalt is a well-known ferrite strengthener,[11] but its strengthening of γ-iron is the new result in the present investigation. This strengthening is more at lower strain rates. The higher activation energy for diffusion of cobalt in γ-iron is likely to be the reason for this high-temperature strengthening effect. The other factors that may contribute to the strengthening by cobalt are its higher atomic diameter (0.251 nm) and a possible decrease in stacking fault energy.

The maraging steel is much stronger than any of the other materials tested. This could be attributed to the higher Co content (~8%) and other minor alloying additions including Ti. At elevated temperatures, the enhanced strength is essentially due to solid solution strengthening by Co.

3.3.2 Kinetic Analysis. The kinetic parameters that represent the hot deformation of all the materials tested in this investigation are listed in Table 4 for the purpose of comparison. The stress exponent, n, is highest for Fe-5Co alloy while the values for other materials are comparable. This result is consistent with the strengthening effect discussed above. The value of n, which is in the range 4.2-5.8, is generally observed

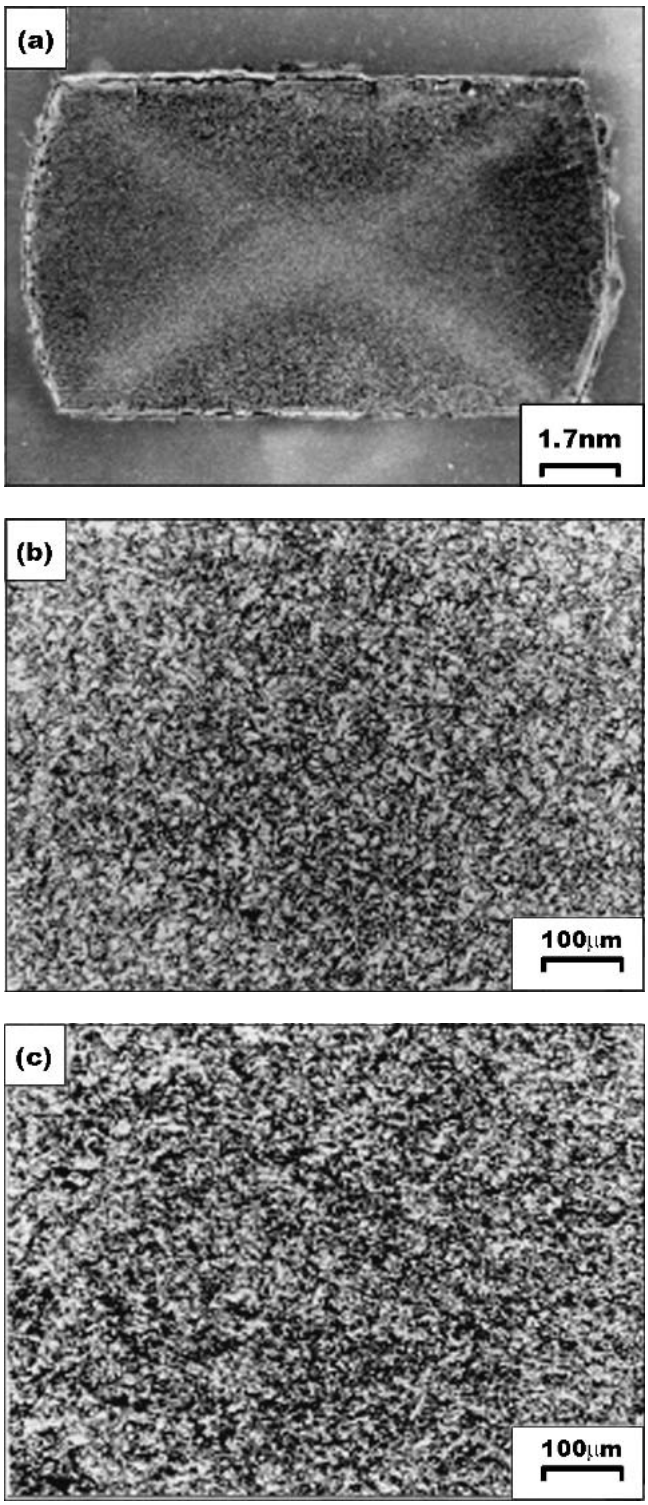

Fig. 16 **(a)** Macrostructure recorded on maraging steel specimen deformed at 950 °C/100 s^{-1}, showing **(a)** localized shear bands and microstructure **(b)** inside and **(c)** outside the band (The compression axis is vertical.)

for DRX process. However, the apparent activation energy for all the alloys and maraging steel is of similar magnitude, which is slightly lower than that obtained for γ-iron. Also, these val-

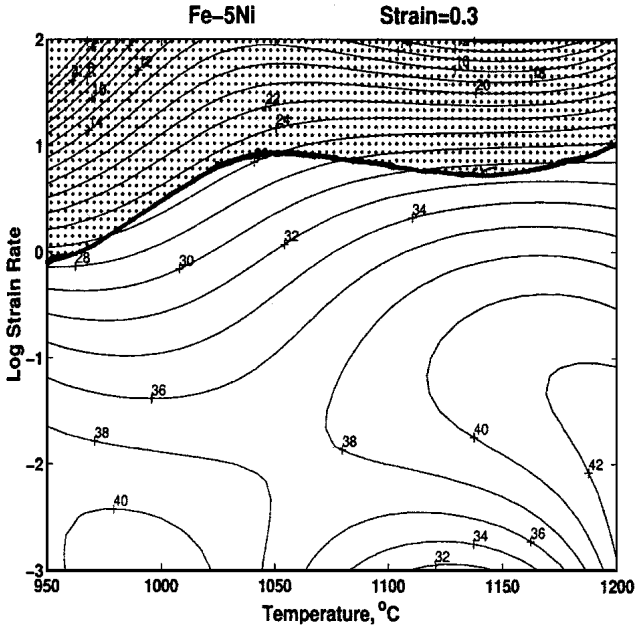

Fig. 17 Processing map obtained for Fe-5Ni alloy at a strain of 0.3. Contour numbers represent percent efficiency of power dissipation. Shaded region corresponds to flow instability.

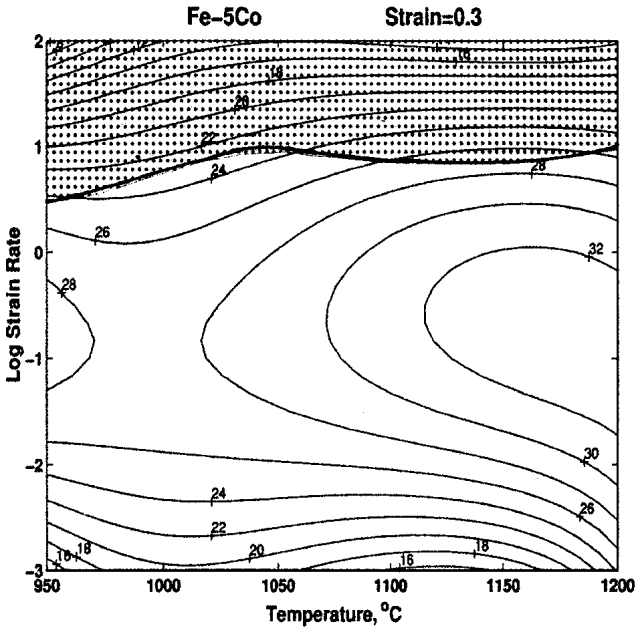

Fig. 18 Processing map obtained for Fe-5Co alloy at a strain of 0.3. Contour numbers represent percent efficiency of power dissipation. Shaded region corresponds to flow instability.

ues are much larger than the corresponding values for diffusion (also given in Table 4). For the DRX process, the apparent activation energy is generally higher than that for self-diffusion since the process involves nucleation and growth, both of which are dependent on the rate of evolution of microstructure during deformation.

3.3.3 Processing Maps. The results from the processing

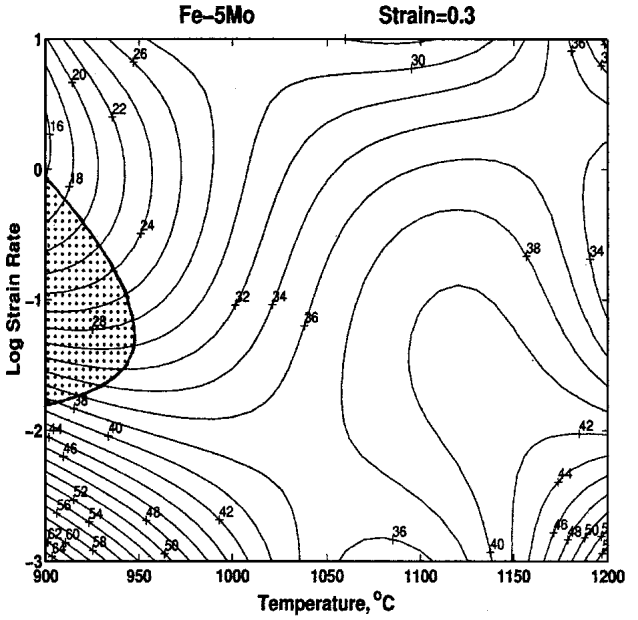

Fig. 19 Processing map obtained for Fe-5Mo alloy at a strain of 0.3. Contour numbers represent percent efficiency of power dissipation. Shaded region corresponds to flow instability.

maps for all the materials tested are shown in Table 4. All the materials exhibited a domain of DRX and the optimum temperature for DRX is generally in the range between 1120-1150 °C. The DRX temperature for Fe-5Co alloy is the same as that for γ-iron but is slightly higher than that for other materials, including maraging steel. However, the optimum strain rates have exhibited considerable differences. The DRX strain rate for γ-iron is the highest, followed in the decreasing order by Fe-5Co, Fe-5Ni, Fe-5Mo, and maraging steel. For example, maraging steel has an optimum strain rate of 0.001 s^{-1}, which is more than two orders of magnitude smaller than that for γ-iron. As regards the peak efficiency of power dissipation in the DRX domain, Fe-5Co gave the lowest value of 32%, followed in the increasing order by γ-iron, Fe-5Mo, Fe-5Ni, and maraging steel. Low stacking fault energy materials like copper and nickel exhibit peak DRX efficiency of the order 32%[12,13] which suggests that the addition of Co to γ-iron lowers its stacking fault energy considerably. The variation of stacking fault energy of γ-iron with the addition of alloying additions has not been measured and such a conclusion is entirely based on η values. However, the higher value for stress exponent and the increased strengthening effect in the Fe-5Co alloy are in support of such a possibility of strengthening by stacking faults.

With regard to the presence of domains other than DRX, the results on processing maps clearly show that in the binary alloys, there is a possibility for the occurrence of wedge cracking at lower strain rates (<0.1 s^{-1}) and temperatures (900-1000 °C). The weakening of grain boundaries at elevated temperatures is caused by the segregation of the alloying elements and promotes the grain boundary sliding process at slow strain rates. When the stress concentration at the triple junctions is not relieved by any of the accommodation processes, wedge

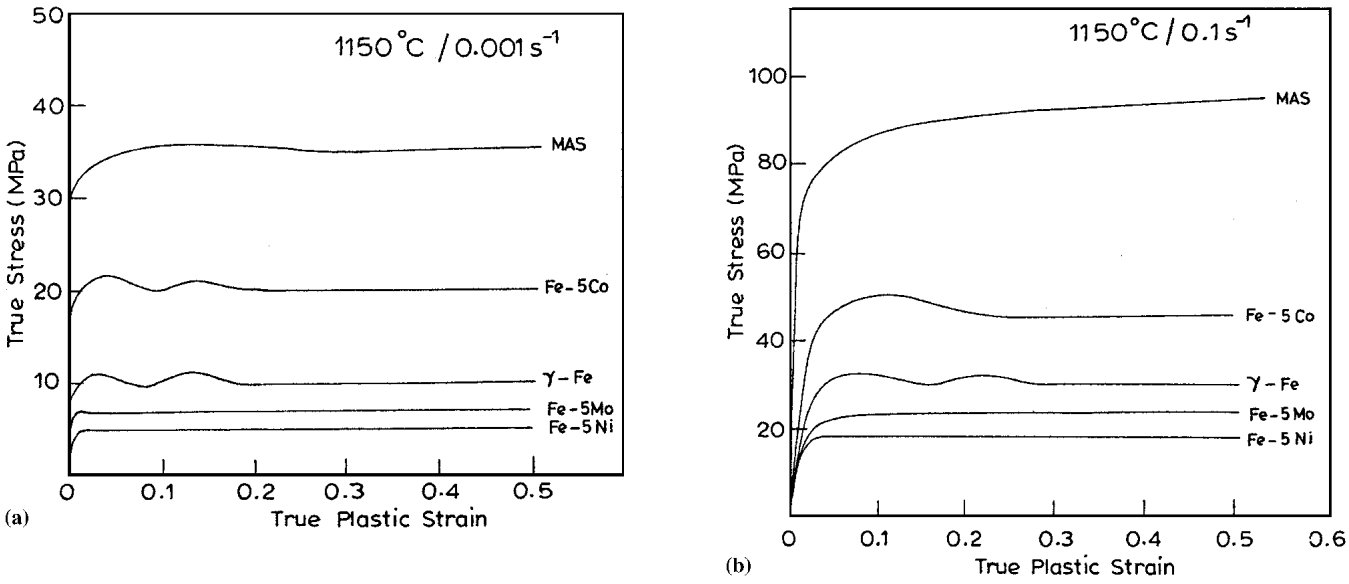

Fig. 20 True stress-true plastic strain curves for γ-iron, Fe-5Ni, Fe-5Co, Fe-5Mo, and maraging steel, obtained at 1150 °C and at a strain rate of **(a)** 0.001 s^{-1} and **(b)** 0.1 s^{-1}

Table 4 Summary of Hot Deformation Results from Kinetic Analysis and Processing Maps on γ-Iron, Fe-5Ni, Fe-5Co, Fe-5Mo, and Maraging Steel

Parameters	γ-Fe	Fe-5Ni	Fe-5Co	Fe-5Mo	Maraging Steel
n	4.5	4	5.8	4.35	4.2
Q, kJ/mol	395	366	350	345	355
Q_D, kJ/mol	286	252	300	252	…
η_{peak}, %	38	42	32	40	44
DRX T, °C	1150	1135	1150	1120	1125
DRX $\dot{\varepsilon}$, s^{-1}	0.3	0.01	0.1	0.01	0.001
Instability regime	950-1200 °C >10 s^{-1}	950-1200 °C >1 s^{-1}	950-1200 °C >10 s^{-1}	~900 °C 0.01 s^{-1}	900-1100 °C >1 s^{-1}
Other mechanisms	DRY η = 33% 950-1000 °C 0.001-1 s^{-1}	Wedge Cracking η = 41% 950-1100 °C 0.001-0.1 s^{-1}	Wedge Cracking η = 32% 950 °C 0.001-0.01 s^{-1}	Super Plasticity η = 54% 1150-1200 °C 0.001-0.1 s^{-1}	…

cracking occurs. However, wedge cracking may be mitigated by faster diffusion rates resulting in superplasticity.

Flow instabilities are present in all the materials when deformed at strain rates higher than 10 s^{-1}, resulting in flow localization and there is significant effect of alloying elements on their occurrence. However, the results on Fe-5Ni alloy indicate that the addition of Ni enhances the regime of flow instability to lower strain rates (1 s^{-1}). Such an effect is also reflected in the behavior of maraging steel.

4. Summary and Conclusions

The hot deformation behaviors of γ-iron, Fe-5Ni, Fe-5Co, Fe-5Mo, and maraging steel have been characterized using isothermal constant true strain rate hot compression tests in the temperature range 900-1200 °C and strain rate range 0.001-100 s^{-1} with a goal of understanding the effect of alloying elements Ni, Co, and Mo on the behavior of γ-iron. Since these are the major alloying elements comprising maraging steel, the study is expected to lead into an understanding of their role in deciding the behavior of maraging steel at elevated temperatures. Such studies will be useful for designing hot working processes like ring rolling, which is a key process for the manufacture of rocket motor casings. The shapes of the stress-strain curves are compared and the constitutive equations data are analyzed using materials models like the kinetic analysis and processing maps. The following conclusions have been drawn from this investigation.

- Gamma iron exhibits dynamic recrystallization and the optimum conditions are 1150 °C and 0.3 s^{-1}. Flow localization occurs at strain rates above 10 s^{-1} and at all temperatures and these conditions of flow instability are not suitable for the hot working of γ-iron.
- Maraging steel also exhibits DRX and the optimum conditions are 1125 °C and 0.001 s^{-1}. Unstable flow manifested as flow localization occurs when maraging steel is deformed at higher strain rates (>1 s^{-1}) below 1075 °C.

- The strain rate conditions for ring rolling of maraging steel represent a process of metadynamic recrystallization resulting in grain sizes finer than those obtained during DRX. The temperature of ring rolling, however, should not be allowed to drop below 1075 °C to obtain controlled microstructures.

References

1. Anon., "*Making Shaping and Treating of Steel,*" H.E. McGannon, ed., United States Steel Corp., Pittsburgh, PA, 1964.
2. Y.V.R.K. Prasad and T. Seshachryulu: "Modeling of Hot Deformation for Microstructural Control," *Intl. Mater. Rev.,* 1998, *43*(6), pp. 243-58.
3. Y.V.R.K. Prasad, H.L. Gegel, S.M. Doraivelu, J.C. Malas, J.T. Morgan, K.A. Lark, and D.R. Barker: "Modeling of Dynamic Materials Behaviour in Hot Deformation: Forging of Ti-6242," *Metall. Trans. A,* 1984, *15,* p. 1883.
4. J.L. Robbins, O.C. Shepard, and O.D. Sherby: "Role of Crystal Structure on the Ductility of Pure Iron at Elevated Temperature," *J. Iron Steel Inst.,* 1961, *199,* p. 175.
5. R.A. Reynolds and W.J. McG. Tegart: "The Deformation of Some Pure Irons by High Speed Torsion Over the Temperature Range 700-1250 °C," *J. Iron Steel Inst.,* 1962, *200,* p. 1044.
6. J.J. Jonas, C.M. Sellars, and J. McG. Tegart: "Strength and Structure Under Hot Working Conditions," *Metall. Rev.* 1969, *14,* p. 1-24.
7. Anon., *Diffusion Data,* F.H. Wohlbier, ed., Ohio Diffusion Info. Centre, P.O. Box 505, CH 4500, Solothurn, Switzerland; Vol. 3, No. 4, 1969, p. 394.
8. Anon., *Diffusion Data,* F.H. Wohlbier, ed., Ohio Diffusion Info. Centre, P.O. Box 505, CH 4500, Solothurn, Switzerland, Vol. 1, No. 3, 1969, p. 280.
9. W. Roberts: in *Deformation Processing and Structure,* G. Krauss, ed., ASM, Metals Park, OH, 1984, p. 109.
10. G.S. Avadhani: "Hot Deformation Mechanisms and Microstructural Evolution During Upset Forging of γ-Fe, Fe-5Ni, Fe-5Co, and Fe-5Mo Alloys and Maraging Steel," Ph.D. Thesis, Indian Institute of Science, Bangalore, India, 2001.
11. M. Srinivas, G. Malkondaiah, and P. Rama Rao: "A First Report on Fracture Toughness of bcc Iron as Influenced by Solutes: Opposite Effects of Silicon and Cobalt," *Bull. Mater. Sci.,* 1988, *11,* p. 329.
12. N. Ravichandran and Y.V.R.K. Prasad: "Influence of Oxygen on Dynamic Re-Crystallization During Hot Working of Polycrystalline Copper," *Mater. Sci. Eng.,* 1992, *A156,* p. 156.
13. Y.V.R.K. Prasad and S. Sasidhara: *Hot Working Guide: A Compendium of Processing Maps,* ASM International, Materials Park, OH, 1997.